Biomaterials Science

Drug loaded multilayered gold nanorods for combined photothermal and chemo-therapy

Journal:	*Biomaterials Science*
Manuscript ID:	BM-ART-12-2013-060323.R1
Article Type:	Paper
Date Submitted by the Author:	25-Jan-2014
Complete List of Authors:	Chen, Haiyan; China Pharmaceutical University, Department of Biomedical Engineering Chi, Xuemei; China Pharmaceutical University, Department of Biomedical Engineering Li, Bowen; University of Washington, Department of Bioengineering Zhang, Min; China Pharmaceutical University, Department of Biomedical Engineering Ma, Yuxiang; China Pharmaceutical University, Department of Biomedical Engineering Achilefu, Samuel; Washington University, Department of Radiology Gu, Yueqing; China Pharmaceutical University, Department of Biomedical

Drug loaded multilayered gold nanorods for combined photothermal and chemo-therapy

Haiyan Chen [a, †] Xuemei Chi [a,b †], Bowen Li [d], Min Zhang [a], Yuxiang Ma [a],

Samuel Achilefu [c], Yueqing Gu[a, *]

[a] Department of Biomedical Engineering, School of Life Science and Technology, State Key Laboratory of Natural Medicines, China Pharmaceutical University, 24 Tongjia Lane, Gulou District, Nanjing 210009, China

[b] Hangzhou Zhongmei Huadong Pharmaceutical Co., Ltd, Hangzhou 311000, China

[c] Department of Radiology, School of Medicine, Washington University, St. Louis, Missouri, USA.

[d] Department of Bioengineering, University of Washington, Seattle, USA

† These authors contributed equally to this work.

*Author to whom correspondence should be addressed:

Prof. Yueqing Gu

Email: guyueqing@hotmail.com

Tel : +86-25-83271080

Fax : +86-25-83271046

Abstract: In this study, AuNRs (AuNRs) were firstly stabilized by hexadecyltrimethylammonium bromide (CTAB) and then coated by two kinds of polyelectrolytes (PE) and BSA to obtain multi-layered AuNRs (AuNRs-PE-BSA). Furthermore, anti-cancer drug doxorubicin (DOX) was encapsulated into AuNRs-PE-BSA by electrostatic force and the nanocomposites formed were named as AuNRs/DOX-PE-BSA. The success of coating was verified by transmission electron microscopy (TEM), zeta potential, gel-electrophoresis and thermogravimetic analysis (TGA). MTT assay indicated that the cytotoxicity of AuNRs decreased dramatically after multi-layers capping. The time-dependent nucleus-targeting capability of AuNRs/DOX-PE-BSA was confirmed in cell affinity evaluations. The in vitro and in vivo experiments demonstrated that AuNRs/DOX-PE-BSA, which combined the photothermal and chemo-therapy for tumor therapy, bears markedly improved curative effect and holds promising prospect in the field of nanomedicine.

Key words: gold nanorod; near infrared; Doxorubicin; thermotherapy; chemotherapy; tumor

1. Introduction

Hyperthermia or thermotherapy, applying heat to selectively eradicate tumor cells, is a kind of non-invasive and widely acknowledged treating method in tumor therapy.[1, 2] In hyperthermia, a variety of sources, such as laser, electromagnetic wave, ultrasound and infrared lamp could induce the increase of localized temperature.[3, 4] Near infrared (NIR) light is poorly absorbed by endogenous chromophores including water, melanin and hemoglobin. Thus, NIR light-activated tumor therapies have attracted extensively attentions[5, 6] Conceivably, the employment of NIR irradiation holds great potential to propel the development of hyperthermia and non-invasive diagnostic techniques.

Gold nanorods (AuNRs) are promising optical contrast agents and NIR photothermal transducers, which is contributed by their well biocompatibility and favorable optical properties.[7, 8] AuNRs have two surface plasmon resonance bands. One is the transverse extinction band (usually around 520 nm), and the other is the longitudinal extinction band (tunable from 600 to 900 nm),[9] which can be adjusted to a desired region by controlling their effective size and aspect ratio (ratio of length to diameter).[10] The excellent surface plasma resonances of AuNRs endow them with the capability of converting light energy to heat with high efficiency when excited by NIR laser. The deep tissue penetration and reduced photo-damage could be simultaneously achieved when NIR laser irradiation is carried out.

Current techniques based on chemical and electrochemical methods have been employed for the synthesis of AuNRs. The most convenient and popular synthesizing

strategy is hexadecyltrimethylammonium bromide (CTAB)-templated growth for AuNRs in aqueous dispersion media.[11, 12] However, CTAB is a well-known toxic cationic surfactant. Therefore, it is essential to develop AuNRs with safe surface coatings. Although PEGylated AuNRs have been reported to perform well in both of in vitro and in vivo tests for their biocompatibility and photothermal effect, their further development was obstructed by the short circulating time in vivo (half-life 1 h).[13] Meanwhile, the facile surface modification of AuNRs by alternately introducing anionic and cationic polyelectrolyte (PE) multilayers[14] could significantly lower the cellular toxicity of AuNRs.[15] Alkilany et al. reported that bovine serum albumin (BSA) from biological media could be adsorbed onto AuNRs, which effectively mediated the receptor-mediated endocytosis due to the cellular recognition of BSA.[16]

Attracted by the lower toxicity of AuNRs in comparison with other inorganic nanomaterials, a lot of researches have been carried out with a focus on the biomedical applications of AuNRs including diagnosis,[17] imaging[18] and photothermal therapy,[19] as well as developing AuNRs as new releasing systems for photoactivated release of biomolecules.[20] These studies revealed the potential to construct a new tumor therapeutic system based on drug-loading AuNRs with simultaneous functions of hyperthermia and chemotherapy. Hence, we are aiming to develop a multifunctional tumor therapeutic system, which utilizes the therapeutic efficacy of AuNRs functioning as photothermal transducers and antitumor drugs that could be released from the system under the excitation of NIR light. Herein, as an attractive and alternative approach to achieve a uniform coating and decrease the bio-toxicity of

CATB-capped AuNRs, the surface of AuNRs was modified with the layer-by-layer coating of PE and BSA. Doxorubicin (DOX) was subsequently encapsulated into multilayered AuNRs by electrostatic force. The in vitro and in vivo therapy effect was comprehensively evaluated among free DOX, AuNRs/DOX-PE-BSA with or without NIR light irradiation to demonstrate the improved curative effect of DOX-loading multilayered AuNRs led by the combination of hyperthermia and chemotherapy.

2. Materials and Methods

2.1 Materials

Chloroauric acid ($HAuCl_4 \cdot 3H_2O$, ≥99.9% purity), CTAB, sodium borohydride ($NaBH_4$), L-ascorbic acid (L-AA), and silver nitrate ($AgNO_3$) were all purchased from Shanghai Chemicals Co. Ltd (Shanghai, China). Sodium poly (styrene sulfonate) (PSS, Mw: 70 kDa), and poly (diallyldimethylammonium chloride) (PDDA, Mw: 15 kDa) were obtained from Sigma-Aldrich (Tianjing China). DOX was purchased from Jiangsu Research Institute (Wuxi, China). 3-(4, 5-diMethylthialzol-2-yl)-2, 5-diphe-nyltetrazolium bromide (MTT), RPMI 1640, fetal bovine serum (FBS), streptomycin, penicillin and trypsin-EDTA were purchased from commercial sources. All chemicals were of analytical reagent grade and used as received without further purification. Deionized water ($18.2M\Omega.cm^{-1}$) was used in all experiments,

2.2 Synthesis of AuNRs capping with PSS, PDDA and BSA

AuNRs were synthesized by an improved seed-mediated growth method.[21] Firstly, CTAB solution (5.0 ml, 0.1 M) was mixed with $HAuCl_4$ (5.0 mL, 0.0005 M). Then,

ice-cold $NaBH_4$ (0.6 mL, 0.1 M) was added under stirring, while the resulting seed solution turned to brownish yellow color. The seed solution was kept at room temperature (25 °C) and used within 5 h. Secondly, the growth solution was prepared as follows: CTAB (100.0 mL, 0.1 M), $HAuCl_4$ (100.0 mL, 0.1 M) and $AgNO_3$ (5.0 ml, 10.0 mM) were gently mixed at 25 °C. Ascorbic acid (1.4 mL, 0.0788 M) was added to the solution, and the solution color changed from dark yellow to colorless. Thirdly, 0.24 mL of the seed solution was added to the growth solution. As-grown AuNRs were further subjected to overgrowth, and the AuNRs with enhanced absorption peak around 765 nm were obtained. After 1 h, the reaction was stopped by centrifugation (12000 rpm, 10 min). The precipitates were collected and re-dispersed in deionized water. Finally, the suspension of AuNRs with the aspect ratio of 3.9 was obtained.

A positively charged CTAB bilayer on the surface of the as-prepared AuNRs served as the basis for layer by layer (LbL) deposition of PE (PSS and PDDA) and BSA. The PSS and PDDA stock solutions were prepared in 1.0 mM NaCl (3.0 mg / mL). 200 μL of PSS stock solution was added into 1.0 mL of the as-prepared AuNRs solution. After gently mixing for 30 min, the excess polymer in the supernatant fraction was removed by centrifugation (14500 rpm, 10 min), and the precipitate was re-dispersed in 1.0 mL of 1.0 mM NaCl solution. PSS-coated rods were incubated with 200 μL of PDDA stock solution for 20 min at room temperature. The rods were then washed by centrifugation (14500 rpm, 10 min) and resuspended in 1.0 mL of NaCl (1.0 mM) solution. The PSS and PDDA adsorption process was repeated once again, and then PE coated multilayered AuNRs (AuNRs-PE) was obtained. Subsequently, the pH of

the resulting rods solution was adjusted to 4.0. Before further coating AuNRs-PE with BSA, the PSS layer was adsorbed onto surface of AuNRs-PE firstly according to the method as mentioned above. 200 μL of BSA aqueous solution (2.0 mg / mL) was then mixed with AuNRs-PE solution and incubated together for 20 min. The rods were then washed by centrifugation (14500 rpm, 10 min) and re-suspended in 1.0 mL of NaCl (1.0 mM) solution. The PSS and BSA absorption process was repeated for another two times. Finally, PE and BSA multilayered AuNRs (AuNRs-PE-BSA) were obtained.

2.3 Preparation of DOX Loaded AuNRs-PE-BSA

For DOX loading, AuNRs-PE-BSA were firstly suspended in PBS solution (pH = 7.4). DOX was then added into AuNRs-PE-BSA solution (2.0 mL) with a final concentration of 50 μg/ml and then stirred for 24 h at 37 °C. During the incubation course, DOX was self-absorbed into the multilayers of AuNRs-PE-BSA by electrostatic interaction. Subsequently, the DOX-loaded AuNRs-PE-BSA (AuNRs/DOX-PE-BSA) was washed by centrifugation (14000 rpm, 10 min) and the surfactant was suspended in PBS solution. The process was repeated for four times. The obtained product was lyophilized and weighted.

2.4 Characterization

2.4.1 Size and Morphology

Transmission electron microscopy (TEM) images of the AuNRs were taken by a JEM-2000 EX II transmission scanning electron microscope (JEOL Company, USA) using an accelerating voltage of 160 kV. The size distribution analysis was performed

by manually measuring the length and width of each rod (at least 200 AuNRs for each sample), and the aspect ratio was also calculated.

2.4.2 Optical properties

The images of rods solution obtained from different synthesis condition were collected by a digital camera at white light. The absorbance spectra of AuNRs, AuNRs-PE and AuNRs-PE-BSA were also acquired by UV-Vis spectrophotometer. AuNRs/DOX-PE-BSA were dispersed in PBS solution with different concentrations (6.0 - 80 μg / mL) and measured by UV-Vis spectrometer at a wavelength of 481.5 nm.

2.4.3 Zeta Potential (ζ)

Zeta Potential of the nanorods was measured using a Zetasizer (Brookhaven Instruments Corporation, US)) at a temperature of 25 °C. All the samples were dispersed in deionized water and the surface charge of the products was investigated by a potential analyzer.

2.4.4 Characterization of BSA Binding

BSA binding was assayed by sodium dodecyl sulfate polyacrylamide gel electrophoresis (SDS-PAGE). Each solution containing AuNRs (1.0 mM) was mixed with loading buffer containing 10 % SDS, 50 % glycerol, 5 % β-mercaptoethanol, 0.5% bromophenol blue and 250 mM Tris-HCl (pH 6.8) and then heated to 95 °C for 5 min. The adsorbed BSA was then identified by electrophoresis with separating gel containing 12 % polyacrylamide.

Thermogravimetric analysis (TGA) of AuNRs-PE-BSA was detected by TG209C

thermogravimetry Analyzer (NETZSCH, Germany). Samples were heated at the scanning rate of 10 K/min over a temperature range from 30 ℃ to 400 ℃.

2.5 Cell studies

2.5.1 Cell culture

The human cell line MCF-7 (breast cancer) was purchased from ATCC. The cell line was cultured at 37 °C in a humidified atmosphere containing 5 % CO_2 in DMEM and RPMI1640 medium supplemented with 10 % fetal bovine serum, 100 U mL^{-1} penicillin, and 100 mg mL^{-1} streptomycin.

2.5.2 Cellular uptake and Cell apoptosis

The affinity of free DOX, AuNRs/DOX-PE and AuNRs/DOX-PE-BSA to cells investigated by laser confocal fluorescence microscopy (LCFM, FV1000, Olympus). Briefly, MCF-7 cells were seeded in LCFM culture dishes (diameter: 35 mm; base thickness: 0.13 mm - 0.17 mm) with a density of 4×10^4 cells/cm^2 and subsequently incubated at 37 ℃ in a humidified atmosphere containing 5 % CO_2. After the confluency of cells was 75 %, the cells were treated with 50 μL of free DOX, AuNRs/DOX-PE and AuNRs/DOX-PE-BSA respectively for 45 min. Subsequently, the cells were washed three times with Dulbecco's phosphate buffered saline (PBS, pH 7.0). For Hoechst staining of the nucleus, the cells were incubated with 50 μL of Hoechst solution (10 μg / mL) for 30 min and then washed by PBS for three times before the subsequent LCFM examination The red fluorescence from DOX was collected, and the excitation light (488 nm) and emission filter (570±15 nm) were used for the fluorescence detection.

In addition, the time-dependent cell uptake study was performed by incubating AuNRs/DOX-PE-BSA with MCF-7 cells at different incubation time (15 min, 35 min and 1 h). The fluorescence images were collected by the same method mentioned above.

To evaluate the therapeutic efficacy of free DOX, AuNRs/DOX-PE-BSA and AuNRs/DOX-PE-BSA (NIR light), the induction of apoptosis in MCF-7 cells was studied by determining the cell number and cell morphology. Specifically, cells were plated at a density of 4×10^4 cells/cm^2 in LCFM culture dish and subsequently incubated under the culture condition for 36 h. The cells were treated with 100 μL of the sample solution (50 μg mL^{-1}) for 20 min. The photothermal treatment was performed using a 765 nm high power multimode pump laser (diameter: 2.0 cm, 1.8 W/cm$^{2)}$. The cells were exposed under the 765 nm laser for 5 min and then washed three times with PBS (pH = 7.0). After another 12 h incubation, the residual cells and the morphological changes were displayed by the differential interference contrast (DIC) mode of LCFM.

2.5.3 Cytotoxicity assay

To evaluate the biotoxicity of AuNRs, AuNRs-PE-BSA and AuNRs/DOX-PE-BSA, MTT assay was conducted on MCF-7 cell line following standard protocols. Cells were plated at a density of 1×10^4 cells per well in 96-well plates. After 24 h incubation, the samples of a wide concentration range (0.005 μg mL^{-1} to 1.0 μg mL^{-1}) were subsequently added into the cells. Each concentration was tested in 6 wells. About 24 h after incubation, each well was replaced and the cells were washed three

times with Dulbecco's phosphate buffered saline (PBS, pH 7.0) before addition of 180 μL of fresh DMEM and 20 μL of MTT solution (5 mg mL^{-1}). After incubation for another 4 h, the medium containing MTT was carefully removed from each well and 150 μL of DMSO was added into each well. The optical density (OD) was measured by a multi-well plate reader.

In addition, the anti-tumor effect of free DOX with and without NIR light irradiation, AuNRs/DOX-PE-BSA with and without NIR light irradiation was estimated and compared following the same procedure mentioned above except that the sample incubation time was set as 4 h. Laser exposure experiments were carried out after the cells were incubated with the sample solutions of a wide concentration range (0.5 μg mL^{-1} to 20.0 μg mL^{-1}) for 4 h. The parameters of light irradiation condition were set as laser (765 nm), time (5 min / well) and power (1.8 W / cm^2) and the cell medium was heated to about 42 °C. The cell viability was calculated by the following equation:

Viable cells (%) = $(OD_{treated}/OD_{control}) \times 100$ %, where $OD_{treated}$ was obtained in the presence of the samples; $OD_{control}$ was obtained from the incubation medium.

2.6 Animal Studies

2.6.1 Animal subjects and tumor model

Normal (Kunming) mice were purchased from Charles River Laboratories (Shanghai, China) for in vivo imaging investigation. All animal experiments were carried out in compliance with the Animal Management Rules of the Ministry of Health of the People's Republic of China (Document NO. 55, 2001) and the

guidelines for the Care and Use of Laboratory Animals of China Pharmaceutical University.

The S180 tumor model for therapy evaluation was established by subcutaneously inoculating S180 cells (~8 $\times 10^6$) into the upper left axillary fossa of the mice (n=48). The mice were investigated when the tumor grew to a diameter of 5 mm.

2.6.2 In vivo imaging

AuNRs/DOX-PE-BSA (0.2 mL, 8 mg/kg) and PBS (0.2 mL) were intratumoral injected into each mouse. The mice were then immobilized on a Lucite jig. The images of the mice were collected at 15 min post-injection by NIR fluorescence imaging system, which is equipped with a 765 nm laser, a high sensitive NIR CCD camera, an 800 nm (± 5 nm) band pass filter and a condenser.

2.6.3 Tissue distribution

After 16 days of intratumoral injection of DOX and AuNRs/DOX-PE-BSA respectively, the mice were sacrificed and the main organs (heart, liver, spleen, lung and kidney) and tumor were collected. The tissues were cut into slices (8 μm thickness) by a freezing microtome (CM1850, Leica) and observed by LCFM immediately. The red fluorescence emitted from DOX was detected.

2.6.4 Therapeutic efficacy

The mice were randomly divided into six groups and then treated with different injections, as follows: (1) PBS (the control group, n = 8); (2) PBS with NIR light excitation (n = 8); (3) DOX (n = 8); (4) DOX with NIR light irradiation (n = 8); (5) AuNRs with NIR light irradiation (n = 8); (6) AuNRs/DOX-PE-BSA with NIR light

irradiation (n = 8). Each mouse underwent 4 intratumorally injection once every three days in 12 days. The tumors were irradiated 1 h post-injection with a 765 nm laser (1.8 W / cm^2) for 5 min in each time. The localized temperature increased to ~ 43 °C. The tumor volume was calculated as length × $(width)^2$ × 1/2.

To further investigate the therapeutic effects of AuNRs/DOX-PE-BSA on S180 tumor bearing mice and its possible toxicity on other organs, the tumors and the organs (heart, liver, spleen, lung and kidney) of the control group and the group treated with PBS, AuNRs-PE-BSA, DOX and AuNRs/DOX-PE-BSA were excised for pathological analysis at 16 day post-injection. The tissues were dissected from the mice, fixed with 10% neutral buffered formalin and embedded in paraffin. The sliced tissues (8 mm) were then stained with Hematoxylin and Eosin (H&E) and examined by Olympus optical microscope.

2.7 Statically Analysis

Significant differences were determined using the Student's t-test where differences were considered significant ($p < 0.05$). All data are expressed as mean ±standard error of the mean.

3. Results and discussion

3.1 Structure, morphology and size

A highlighted feature of plasmonic nanoparticles (Au, Ag, Cu) is their structural-depending optical properties, which facilitates tailoring the longitudinal surface plasmon resonance (LSPR) of AuNRs to a desirable wavelength with optimal light penetration for in vivo applications. Meanwhile, anti-cancer drugs could be

loaded into the multi-layers of AuNRs. Thus, drug loaded AuNRs were favorable nanocomposites for combinational photo-thermal therapy and chemotherapy of tumors.

The synthesis routine of DOX loaded multilayered AuNRs is illustrated in Fig. 1. AuNRs were firstly coated with PE (PSS and PDAC) through LbL assembly method. BSA was selected to further capping AuNRs-PE to form AuNRs-PE-BSA. Anti-cancer drug, DOX, was finally loaded to AuNRs-PE-BSA by self-absorption process.

The white light images of AuNRs solutions are shown in Fig. 2A, where a is the seed solution; b is Au nanoparticels solution; c to e are the solutions of AuNRs with different aspect ratios. Fig. 2B is the white light images of AuNRs with LSPR bands at 765 nm (a) and 808 nm (b), respectively. The as-prepared AuNRs before and after centrifugation were also characterized by TEM (Fig. 2C): (a) there are a lot of spherical Au nanoparticles contained in the sample of AuNRs before post-synthesis centrifugation; (b-d) the post-processing AuNRs with different magnification time (× 50000, × 75000 and × 100000) are in unifrom size and morphology. The average aspect ratio of AuNRs is about 4 (length/diameter = ~49/12 in nm).

The absorbance spectra of AuNRs change as a function of AgNO3 volume, aspect ratio, and reaction time (Figure S1 and Figure S2). these results verified previously published literature [22-25]. The experimental conditions for the synthesis of well-defined AuNRs are often difficult to control. Thus, the post-synthesis separation is necessary for the preparation of nanoparticles with monodispersity and uniform size.

Based on their shape-dependent sedimentation behavior, Sharma et al utilized theoretical analysis and experiments to demonstrate the viability of using centrifugation to separate colloidal AuNRs from a mixture of nanorods and nanospheres.[26] Xiong et al reported that relatively heavier but longer and thinner rods could precipitate slower than certain size of lighter spheres, and AuNRs with diverse aspect ratios can be separated using density-gradient centrifugation.[27] Correspondingly, the post-synthesis centrifugation method was adopted in our experiments to purify the as-prepared AuNRs and the effectiveness of the reported means was validated.

Due to the toxicity of surfactants such as CTAB, SDS and so on, much effort has been devoted to decreasing the toxicity and improving the biocompatability of AuNRs. CTAB molecules on the surface of the gold nanorods are exchangeable with similar surfactants that have a positively charged headgroup and surfactant polymerization on the surface of the gold nanorods enhances both the stability and biocompatibility of these nanomaterials.[28] Ye et al.[29] proposed an improved method for the synthesis of colloidal AuNRs by using aromatic additives (5-bromosalicylic acid or 2,6-dihydroxybenzoic acid). Thus, the concentration of CTAB surfactant decreased to ~0.05 M. Choi et al.[30] validated that the use of heat or acid could completely remove CTAB from the synthesized Au nanorods while their stability was still maintained by pluronic F-127. Therefore, the well-established synthetic protocols of CTAB stabilized AuNRs could be further improved by replacing CTAB with lower toxic or non-toxic surface stabilizer.

3.2 The multi-layers coating on the surface of AuNRs

Direct visualization of the layers coating on AuNRs can be achieved by TEM observation. Fig. 3A shows the high-resolution TEM micrographs of the AuNRs coated by different layers. After four layers of polymer coating (PSS+PDDA+PSS+PDDA), the thickness of layers was approximate to 2 nm. The layer thickness increased to ～6 nm for AuNRs-PE-BSA. The UV-Vis-IR absorbance spectra of the AuNRs coated by different layers are shown in Fig. 3B. The absorption peak around 520 nm is ascribed to the transverse surface plasmon band of the nanorods, and the absorption peak around 765 nm is attributed to the LSPR band. The LSPR peak was slightly blue-shifted as the nanorods were coated with the first four layers of polymer. However, the LSPR maximum reverted to the original position (765 nm) when AuNRs-PE-BSA was formed.

Zeta potential is usually used to confirm the surface charge and stability of nanoparticles in solution. The sequential absorption of oppositely charged molecules onto nanorods' surfaces reversed the charge of nanorods after each deposition step. As shown in Fig. 4A, the zeta potential of AuNRs is ca.+38.2 mV due to the presence of a bilayer of CTAB on the nanorods surface. PDDA-coated AuNRs are positively charged (step 2, 4) while the PSS-coated AuNRs are negatively charged (step 1, 3, 5, 7, 9). After incubated with BSA solution in acidic condition, surface charges of all AuNRs were found to become positive immediately (step 6, 8 10). It can be clearly seen that the charge reversed upon sequential molecular adsorption. SDS-PAGE measurement was employed to evaluate the amount of BSA adsorbed by each sample

(Fig. 4B). The BSA adsorption was reflected by the bands intensity in the SDS-PAGE gel. List 1 to 5 is corresponding to marker, AuNRs-PE, AuNRs, AuNRs-PE-BSA and BSA, respectively. Obviously, no BSA bands appeared in AuNRs-PE or AuNRs. The bands of gel electrophoresis were semi-quantified using Scion Image software. The band area of the BSA control is 46110 (pixel), and the band area of BSA adsorbed on AuNRs-PE-BSA is 25476 (pixel). This indicated that AuNRs-PE have strong capability to adsorb BSA, which is relative to the easy internalization by cells. TGA curve (Fig. 4C) shows a significant weight loss of AuNRs-PE-BSA (25.2 %) from 30 °C to 400 °C, which could be attributed to the decomposition of the layers as the heating temperature increased.

AuNRs-PE-BSA was prepared by a versatile LbL ssembly approach. PE coating of gold nanoparticles has been studied specifically by Caruso and co-workers, [31, 32] who validated that the polymers should be flexible with a chain length comparable to the dimensions of the nanoparticles. Gittins et al. proved that a low salt concentration (1 mM) and a polymer of 15-20 kDa are ideal for coating of nanoparticles with a size of ~30 nm.[33] As the AuNRs dimension in our case is 50-60 nm in length, we chose the polymers with Mw = 15000-70000 g/mol and salt concentration =1 mM). Alkilany et al reported that BSA from the growth media were found to adsorb on gold nanoparticles and convert the surface charge of nanoparticles to that of BSA, which may facilitate the cellular uptake of nanomaterials via receptor-mediated endocytosis.[16] Furthermore, there are at least four known receptors on cell surface that can independently bind with BSA alone and then endocytose it into cells.[34] Therefore,

further BSA absorption is favorable to achieve uniform coating and efficient cell uptake.

The as-prepared positively charged AuNRs were firstly coated with a layer of anionic polymer (PSS). Multilayers of oppositely charged polymers were formed based on LbL assembly (PSS-PDDA-PSS-PDDA). BSA and PSS were then adsorbed sequentially onto the nanorods' surface Caruso et al. utilized analytical ultracentrifugation method to characterize the polymer-coating nanorods.[35] Gole et al observed the PE-coated AuNRs by TEM and SEM detection.[36] Multilayer growth can also be monitored by UV-Vis spectroscopy that determines cumulative absorption attributed to stepwise deposition of UV-active colloids.[37] Accordingly, TEM measurement and absorbance spectra were also employed in this study to characterize AuNRs, AuNRs-PE and AuNRs-PE-BSA. A blue-shift in the gold nanoparticles plasmon band resulted from polymer unwrapping was reported by Gittins et al.[38] Chen et al also found that the longitudinal plasmon band of CTAB-capped AuNRs peak would slightly blue-shift to 790 nm from 800 nm after PSS substitution.[39] However, the blue-shift of LSPR maximum did not appear for AuNRs-PE-BSA, suggesting that BSA and PE were wrapped on the surface of the AuNRs. In addition, zeta potential, SDS-PAGE measurement and TGA analysis further confirmed the multi-layer coating on the surface of AuNRs-PE-BSA.

The LbL self-assembly of multiple layers on nanoparticles resulted in the production of multifunctional hybrid carrier systems for probes, drugs, sensors, enzymes and other multiple components.[40, 41] Ma et al. loaded anti-cancer drugs into

the mesopores of AuNRs-capped magnetic core/mesoporous silica shell nanoellipsoids, demonstrating the advantages of this delivery system in cancer therapy over conventional individual thermo-therapeutic system.[42] Recently, AuNRs and Au nanoparticles were successfully conjugated with hydrophilic photosensitizer to achieve synergistic therapy by photodynamic therapy (PDT) and photothermal therapy (PTT).[43] In this work, anti-cancer drug (DOX) was self-adsorbed into the multi-layers by electrostatic interaction. The loading process was simple, facile and transient. Thanks to the BSA layer, the effective charge on the surface of AuNRs-PE-BSA was stable in the surrounding environment, which improved the drug loading efficiency and cell affinity of the nanorods.

3.3 The distinct cell nucleus affinity of AuNRs/DOX-PE-BSA

Fig. 5A shows the LCFM images of MCF-7 cells, which had been incubated with DOX, AuNRs/DOX-PE and AuNRs/DOX-PE-BSA for 45 min, and then been marked with Hoechst for nuclei staining specifically. In line with the intensity of red fluorescence, only a small quantity of free DOX and AuNRs/DOX-PE bound to the cell membrane and little drug arrived at the cytoplasm in the short incubation time. By contrast, much stronger intensity of red fluorescence on the cell membrane was detected among the cells incubated with AuNRs/DOX-PE-BSA. Moreover, it is noteworthy that red fluorescence of DOX was abundant not only in cytoplasm but also in cell nucleus. BSA is the main protein component in the serum-containing media. BSA alone has at least four known cell surface receptors that can independently bind and endocytose it into cells.[44] BSA adsorbed on the surface of

AuNRs endows the nanorods with the physiochemical characteristics of biological macromolecules. Accordingly, AuNRs/DOX-PE-BSA exhibited much faster endocytosis via receptor mediation. The results also suggest that physiochemical surface property of nanomaterials is a determinant factor for their behavior in biological system. Such changes should be taken into consideration when exploiting the biological application of nanoparticles.

To further examine the cell nucleus affinity of AuNRs/DOX-PE-BSA, the LCFM images of MCF-7 cells incubated with AuNRs/DOX-PE-BSA at different time intervals (15 min, 35 min and 1 h) were collected (Fig. 5B). A time-dependent nucleus-targeting capability of AuNRs/DOX-PE-BSA was demonstrated. The strongest red fluorescence in nucleus could be observed among the cells treated with AuNRs/DOX-PE-BSA for 60 min. Alkilany et al. [16] demonstrated that the amount of BSA adsorbed on AuNRs had a positive correlation with the capacity of AuNRs to enter cells. The adsorbed BSA (or other serum proteins) may facilitate the uptake of nanomaterials via receptor-mediated endocytosis. It is well known that the intracellular targeting location of DOX is the nucleus.[45] Then anti-cancer efficacy of DOX can be enhanced by their effective delivery into cancer cells as well as the high accumulation in the nucleus.

3.4 The fine combined therapeutic efficacy of AuNRs/DOX-PE-BSA on cells

Fig. 6A manifests a slightly dose-dependent reduction in MTT absorbance for the cells incubated with AuNRs, AuNRs-PE-BSA and AuNRs/DOX-PE-BSA, respectively. The cell viability percentage for AuNRs was 65 % at lower dose (0.1

μg/mL), and reduced to 45 % at high dose (1.0 μg/mL). AuNRs-PE-BSA caused a minor reduction in cell viability (> 80%) even at the highest dose (1.0 μg/mL). After being loaded with DOX, AuNRs/DOX-PE-BSA led the viability of treated cells to decreasing to 52 % at high dose (1.0 μg/mL). A distinction of cell viability exists between AuNRs, AuNRs@PE and AuNRs/DOX@PE as the incubation concentration is larger than 0.1 μg/mL.

To compare the combined therapy with each single therapy, the inhibition rates of free DOX, AuNRs/DOX-PE without laser irradiation, as well as AuNRs/DOX-PE-BSA with laser irradiation were measured by MTT assay (Fig. 6B). The viability of the cells treated with AuNRs/DOX-PE-BSA under the excitation of NIR is the lowest (26 % at a concentration of 20 μg/mL). Free DOX with or without light irradiation shows similar cell viability at different concentrations. For the treatment of AuNRs/DOX-PE without NIR light excitation, the cell viability is higher than 80 % even at the highest dose (20 μg/mL). The combined chemotherapeutic and thermotherapeutic effect of AuNRs/DOX-PE-BSA under NIR light was also observed by the DIC mode of LCFM, which was shown in Fig. 6C. After light irradiation, cell apoptosis was obviously observed among the cells incubated with AuNRs/DOX-PE-BSA. Specifically, most of the cells were washed away by PBS buffer solution, and the cells in the field of vision were scanty, comparable to those incubated with free DOX. By contrast, while some cells became rounded and were detached from the dish, a relatively large number of cells stilled retained in AuNRs/DOX-PE-BSA incubated dish (without laser irradiation) after PBS washing.

All the results revealed the preferable therapeutic effects of AuNRs/DOX-PE-BSA combined with NIR light irradiation.

The toxicity of CTAB-encapsulated AuNRs was mainly caused by CTAB on the surface of AuNRs.[46] Alkilany et al' work has demonstrated a shape-independent but coating-dependent cytotoxicity of AuNRs,[16] in which the inhibition rates of AuNRs reduced dramatically after being coated with multi-layers of PE and BSA. However, the cytotoxicity displayed by AuNRs/DOX-PE-BSA under the excitation of NIR light was similar to that of free DOX though the amount of DOX encapsulated in AuNRs/DOX-PE-BSA was much lower than that of free DOX. Therefore, the meliority of synergistic anti-cancer therapeutic effect of chemo- and thermal therapy was demonstrated in AuNRs/DOX-PE-BSA with NIR light irradiation at the cell level.

3.5 The NIR light absorption capability of AuNRs/DOX-PE-BSA in tumor-bearing mouse model

To demonstrate the high LSPR effect of AuNRs/DOX-PE-BSA, the normal mice was injected via axillary with 0.2 mL of AuNRs/DOX-PE-BSA and then exposed to laser irradiation. The NIR fluorescence images of the mice for control (before injection) and the mice treated with AuNRs/DOX-PE-BSA were displayed respectively (Fig. 7A). It is easy to notice a deep black circle region in the mouse axillary fossa, which was ascribed to the high NIR light absorption of the nanocomposites.

The tissue distribution of DOX and AuNRs/DOX-PE-BSA after 16 days of

intratumoral injection is indicated in Fig. 7B. The red fluorescence was absent in liver, spleen and kidney, and the fluorescence was only observed from heart and tumor in both of the two groups. The red fluorescence observed from heart of DOX treated mice was obviously stronger than that of AuNRs/DOX-PE-BSA treated group. The result implied that the free DOX was prone to entering into blood circulation even if they were located in the interstitial space of the tumor at the initial time.

The LSPR band of AuNRs is around 765 nm. This NIR absorption peak enabled AuNRs to have strong absorption under 765 nm laser irradiation, which was indicated by the in vivo optical images of the mice treated by AuNRs/DOX-PE-BSA via intratumoral injection. Owing to the enhanced permeability and retention (EPR) effect of tumors, nanoparticles have longer retention time in tumors than that in normal tissues. Moreover, the EPR effect has been proved to strongly associate with the biophysicochemical properties of the nanoparticles [47] meaning that non-targeted nanoparticles can be engineered to accumulate specifically in tumor sites by optimizing their biophysicochemical properties. In this study, BSA layer may contibuted to the long retention time of AuNRs/DOX-PE-BSA in the tumor. In comparison with the biodistribution of DOX in S180 tumor-bearing mice, weaker fluorescence in the heart and stronger fluorescence in the tumor were the characters of mice treated by AuNRs/DOX-PE-BSA, which could be distinctly expounded by the nonspecifically tumor targeting efficacy of AuNRs/DOX-PE-BSA.

3.6 The preferable therapeutic efficacy of AuNRs/DOX-PE-BSA in tumor-bearing mice

The synergistic thermo- and chemo-therapy effect on S180 tumor-bearing mice was investigated. As shown in Fig. 8A, the tumor volume of the mice treated with AuNRs/DOX-PE-BSA coupled with NIR light irradiation increased much more slowly than that of other groups (PBS, PBS with light excitation, free DOX with or without light irradiation and AuNRs-PE-BSA with laser excitation) within 16 days. In comparison, the tumor volume of the mice treated with free DOX increased faster than that of the synergistic therapy group but slower than that of the thermotherapy group. And there is no significant tumor volume difference between the mice treated with free DOX with or without NIR light irradiation.

Tumor sections stained by H&E at 16 day post-injection were histological examined as shown in Fig. 8B. Significant necrosis appeared in groups treated by DOX and AuNRs/DOX-PE-BSA (NIR light irradiation), while only little necrosis was observed in the tumor tissues belonging to the mice treated by AuNRs-PE-BSA (NIR light irradiation). Almost no damage appeared in the group treated by PBS. Moreover, larger necrosis region with pathological calcification could be observed in the tumors of synergistic treatment group in comparison with the DOX group, further confirming the superiority of the synergistic therapeutic effect of AuNRs/DOX-PE-BSA combined with NIR light. In addition, there were no signs of degenerative and necrotic changes of the parenchymatous cells, interstitial proliferation or inflammatory reaction in the organs (heart, liver, spleen, lung and kidney) for the mice treated with AuNRs/DOX-PE-BSA and PBS (Fig. 8C).

An enhanced anti-cancer efficacy was exhibited by the combination of chemo- and

thermotherapy in recent clinic therapy investigations. Some researchers utilized mesoporous silica as a carrier for the co-delivery of gold nanoparticles and drugs to the targeted tumor, resulting in an apparently enhanced therapeutic efficacy compared with the therapeutic effect of single treatment.[48] Herein, the multi-layered AuNRs were non-covalently conjugated with anti-cancer drug, and a superior therapeutic effect was achieved under NIR light irradiation. The dosage of DOX could be substantially lowered by simply heating the tumor up to ~ 43°C, which was contributed by the synergistic therapeutic effect of AuNRs/DOX-PE-BSA combined with NIR light, and in this way both the dosage-limiting toxicity of the drug and tissue damage by single thermal therapy could be effectively avoided.

4. Conclusion

In summary, multi-layer coated and DOX-loaded AuNRs-PE-BSA, as multifunctional nanomaterials for in vivo combined thermo- and chemotherapy, were prepared via a facile approach mainly based on electrostatic adsorption. Surface modification with BSA improved the biocompatibility, promoted the endocytosis of nanocomposites and provided desirable layers to carry anti-caner drugs. As the cell internalization of nanoparticles was proved to be surface-chemistry-dependent, AuNRs/DOX-PE-BSA showed a facilitated cellular uptake，which was favorable to enhance its anti-tumor effect at cell levels. Furthermore, due to the deep tissue penetration of NIR light and the high LSPR absorbance of AuNRs, the in vivo synergistic thermotherapy and chemotherapy effect of AuNRs/DOX-PE-BSA was perfectly embodied on S180 tumor-bearing mouse model. Such a multifunctional drug

delivery system showed apparent superiority in cancer therapy over conventional individual themo- or chemo-therapeutic system, demonstrating a promising prospect for combined anti-cancer therapeutic techniques.

Acknowledgment

The authors are grateful to Natural Science Foundation Committee of China (NSFC 81371684, 81000666, 81220108012, 61335007, 81171395 and 81328012)) and the Program for New Century Excellent Talents (NCET) in University of the Ministry of Education of China for their financial support.

Reference

1 Tu, J.; Hwang, J. Ha.; Chen, T.; Fan, T.; Guo, X.; Crum, L. A. Controllable in vivo hyperthermia effect induced by pulsed high intensity focused ultrasound with low duty cycles. *Appl. Phys. Lett.* **2012,** *101*, 124102-124106.

2 Galldiks, N.; Tempelhoff, W. Von.; Kahraman, D.; Kracht, L. W.; Vollmar, S.; Fink, G. R. 11C-methionine positron emission tomographic imaging of biologic activity of a recurrent glioblastoma treated with stereotaxy-guided laser-induced interstitial thermotherapy. *Mol. Imaging.* **2012,** *11*, 265-271.

3 Roder, P. B.; Pauzauskie, P. J.; Davis, E. J. Nanowire heating by optical electromagnetic irradiation. *Langmuir.* **2012,** *28*, 16177-16185.

4 Yang, R.; Li, X.; Song, A.; He, B.; Yan, R. Three-dimensional noninvasive ultrasound Joule heat tomography based on the acousto-electric effect using unipolar pulses: a simulation study. *Phys. Med. Biol*. **2012,** *57*, 7689-7708.

5 Yuan, L.; Lin, W.; Yang, Y.; Chen, H. A unique class of near-infrared functional fluorescent dyes with carboxylic-acid-modulated fluorescence ON/OFF switching: rational design, synthesis, optical properties, theoretical calculations and applications for fluorescence imaging in living animals. *J. Am. Chem. Soc.* **2012,** *134*, 1200-1211.

6 Jayakumar, M. K.; Idris, N. M.; Zhang, Y. Remote activation of biomolecules in deep tissues using near-infrared-to-UV upconversion nanotransducers. *Proc. Natl. Acad. Sci. U. S. A.* **2012,** *109*, 8483-8488.

7 Huang, X. H.; El-Sayed, I. H.; Qian, W.; El-Sayed, M. A. Cancer cell imaging and photothermal therapy in the near-infrared region by using AuNRs. *J. Am. Chem. Soc.* **2006,** *128*, 2115-2120.

8 Zhang, Y.; Wang, Q. Magnetic-plasmonic dual modulated FePt-Au ternary heterostructured nanorods as a promising nano-bioprobe. *Adv. Mater.* **2012,** *24*,

2485-2490.

9 Lee, K. S.; El-Sayed, M. A. Gold and Silver Nanoparticles in Sensing and Imaging: Sensitivity of Plasmon Response to Size, Shape, and Metal Composition. *J. Phys. Chem.* **2006,** *110*, 19220-19225.

10 Lee, K. S.; El-Sayed, M. A. Dependence of the Enhanced Optical Scattering Efficiency Relative to That of Absorption for Gold Metal Nanorods on Aspect Ratio, Size, End-Cap Shape, and Medium Refractive Index. *J. Phys. Chem. B.* **2005,** *109*, 20331-20338.

11 Mieszawska, A. J.; Jalilian, R.; Sumanasekera, G. U.; Zamborini F. P. Synthesis of gold nanorod/single-wall carbon nanotube heterojunctions directly on surfaces. *J. Am. Chem. Soc.* **2005,** *127*, 10822-10823.

12 Xiang, Y.; Wu, X.; Liu, D.; Li, Z.; Chu, W.; Feng, L. Gold nanorod-seeded growth of silver nanostructures: from homogeneous coating to anisotropic coating. *Langmuir.* **2008,** *24,* 3465-3470.

13 Choi, W. I.; Kim, J. Y.; Kang, C. Tumor regression in vivo by photothermal therapy based on gold-nanorod-loaded, functional nanocarriers. *ACS nano*. **2011,** *5*, 1995-2003.

14 Alkilany, A. M.; Shatanawi, A.; Kurtz, T.; Caldwell, R. B.; Caldwell, R. W. Toxicity and cellular uptake of AuNRs in vascular endothelium and smooth muscles of isolated rat blood vessel: importance of surface modification. *Small.* **2012,** *8*, 1270-1278.

15 Huang, H. C.; Barua, S.; Kay, D. B.; Rege, K. Simultaneous enhancement of photothermal stability and gene delivery efficacy of AuNRs using polyelectrolytes. *ACS. Nano.* **2009,** *3*, 2941-2952.

16 Alkilany, A. M.; Nagaria, P. K.; Hexel, C. R.; Shaw, T. J.; Murphy, C. J.; Wyatt, M.

D. Cellular Uptake and Cytotoxicity of AuNRs: Molecular Origin of Cytotoxicity and Surface Effects. *Small.* **2009,** *5*, 701-708.

17 Zhang, Y.; DaSilva, M.; Ashall, B.; Doyle, G.; Zerulla D.; Sands, T. D.; Lee, G. U. Magnetic manipulation and optical imaging of an active plasmonic single-particle Fe-Au nanorod. *Langmuir.* **2011,** *27*, 15292-15298.

18 Jokerst, J. V.; Thangaraj, M.; Kempen, P. J.; Sinclair, R.; Gambhir, S. S. Photoacoustic imaging of mesenchymal stem cells in living mice via silica-coated gold nanorods. *ACS. Nano.* **2012,** *6*, 5920-5930.

19 Wang, J.; Zhu, G.; You, M.; Song, E.; Shukoor, M. I.; Zhang, K. Assembly of aptamer switch probes and photosensitizer on gold nanorods for targeted photothermal and photodynamic cancer therapy. *ACS. Nano*. **2012,** *6*, 5070-5077.

20 Wijaya, A.; Schaffer, S. B.; Pallares, I. G.; Hamad-Schifferli, K. Selective release of multiple DNA oligonucleotides from gold nanorods *ACS. Nano*. **2008,** *3*, 80-86.

21 Huang, X.; Neretina, S.; El-sayed, M. A. gold nanorods: from synthesis and properties to biological and biomedical applications. *Adv Mater.* **2009,** *21*, 4880-4910.

22 Kim, F.; Song, J. H.; Yang, P. Photochemical synthesis of gold nanorods. *J. Am. Chem. Soc.* **2002,** *124*, 14316-14317.

23 Jana, N. R.; Gearheart, L.; Murphy, C. J. Wet Chemical Synthesis of High Aspect Ratio Cylindrical Gold Nanorods. *J. Phys. Chem. B.* **2001,** *105,* 4065-4067.

24 Gole, A.; Murphy, C. J. Seed-Mediated Synthesis of Gold Nanorods: Role of the Size and Nature of the Seed. *Chem. Mater.* **2004,** *16,* 3633-3640.

25 Vigderman, Leonid.; Khanal, B. P.; Zubarev, E. R. Functional Gold Nanorods: Synthesis, Self-Assembly, and Sensing Applications. *Adv Mater.* **2012,** *24*, 4811-4841.

26 Sharma, V.; Park, K.; Srinivasarao, M. Shape separation of AuNRs using centrifugation. *Proc. Natl. Acad. Sci. U. S. A.* **2009,** *106*, 4981-4985.

27 Xiong, B.; Cheng, J.; Qiao, Y.; Zhou, R.; He, Y.; Yeung, E. S. Separation of nanorods by density gradient centrifugation. *J. Chromatogr. A.* **2012,** *1218*, 3823-3829.

28 Alkilany, A. M.; Nagaria, P. K.; Wyatt, M. D.; Murphy, C. J. Cation exchange on the surface of gold nanorods with a polymerizable surfactant: polymerization, stability, and toxicity evaluation. *Langmuir.* **2010,** *26,* 9328-9333.

29 Ye, X.; Jin, L.; Caglayan, H.; Chen, J.; Xing, G.; Zheng, C.; Doan-Nguyen, V.; Kang Y.; Engheta, N.; Kagan, C. R.; Murray, C. B. An improved size-tunable synthesis of monodisperse AuNRs through the use of aromatic additives. *ACS. Nano.* **2012,** *6*, 2804-2817.

30 Choi, B. S.; Iqbal, M.; Lee, T.; Kim, Y. H.; Tae, G. Removal of cetyltrimethylammonium bromide to enhance the biocompatibility of Au nanorods synthesized by a modified seed mediated growth process. *J. Nanosci. Nanotechnol.* **2008,** *8*, 4670-4674.

31 Cho, J.; Quinn, J. F.; Caruso, F. Fabrication of polyelectrolyte multilayer films comprising nanoblended layers. *J. Am. Chem. Soc.* **2004,** *126*, 2270-2271.

32 Blomberg, E.; Poptoshev, E.; Claesson, P. M.; Caruso, F. Surface interactions during polyelectrolyte multilayer buildup. 1. Interactions and layer structure in dilute electrolyte solutions. *Langmuir.* **2004,** *20*, 5432-5438.

33 Gittins, D. I.; Caruso, F. Tailoring the polyelectrolyte coating of metal nanoparticles. *The Journal of Physical Chemistry B*, **2001,** *105*, 6846-6852.

34 Schnitzer, J. E.; Oh, P. Albondin-mediated capillary permeability to albumin. Differential role of receptors in endothelial transcytosis and endocytosis of native and

modified albumins. *J. Biol. Chem.* **1994,** *269*, 6072-6082.

35 Mayya, K. S.; Schoeler, B.; Caruso F. Preparation and Organization of Nanoscale Polyelectrolyte-Coated Gold Nanoparticles. *Adv. Funct. Mater.* **2003,** *13*, 183-188.

36 Gole, A.; Murphy, C. J. Polyelectrolyte-Coated AuNRs: Synthesis, Characterization and Immobilization. *Chem. Mater.* **2005,** *17*, 1325-1330.

37 Picart, C.; Schneider, A.; Etienne, O.; Mutterer, J.; Schaaf, P.; Egles, C. Controlled degradability of polysaccharide multilayer films in vitro and in vivo. *Adv. Funct. Mater.* **2005,** *15*, 1771-1780.

38 Gittins, D. I.; Caruso, F. Tailoring the polyelectrolyte coating of metal nanoparticles. *J. Phys. Chem. B.* **2001,** *105*, 6846-6852.

39 Chen, C. L.; Kuo, L. R.; Chang, C. L.; Hwu, Y. K.; Huang, C. K.; Lee, S. Y. In situ real-time investigation of cancer cell photothermolysis mediated by excited gold nanorod surface plasmons. *Biomaterials.* **2010,** *31*, 4104-4112.

40 Liang, P.; Zhao, D.; Wang, C. Q.; Zong, J. Y.; Zhuo, R. X.; Cheng, S. X. Facile preparation of heparin/CaCO(3)/CaP hybrid nano-carriers with controllable size for anticancer drug delivery. *Colloids. Surf. B. Biointerfaces.* **2013,** *102*, 783-788.

41 Zhao, E.; Zhao, Z.; Wang, J.; Yang, C.; Chen, C.; Gao, L. Surface engineering of gold nanoparticles for in vitro siRNA delivery. *Nanoscale.* **2012,** *4*, 5102-5109.

42 Ma, M.; Chen, H.; Chen, Y.; Wang, X.; Chen, F.; Cui, X. Au capped magnetic core/mesoporous silica shell nanoparticles for combined photothermo-/chemo-therapy and multimodal imaging. *Biomaterials.* **2012,** *33*, 989-998.

43 Kuo, W. S.; Chang, Y. T.; Cho, K. C.; Chiu, K. C.; Lien, C. H.; Yeh, C. S. Gold nanomaterials conjugated with indocyanine green for dual-modality photodynamic and photothermal therapy. *Biomaterials.* **2012,** *33*, 3270-3278.

44 Schnitzer, J. E.; Oh, P.; Pinney, E.; Allard, J. Filipin-sensitive caveolae-mediated

transport in endothelium: reduced transcytosis, scavenger endocytosis, and capillary permeability of select macromolecules. *J Cell Biol.* **1994,** *127,* 1217-1232.

45 Laginha, K. M.; Verwoert, S.; Charrois, G. J,.; Allen, T. M. Determination of doxorubicin levels in whole tumor and tumor nuclei in murine breast cancer tumors. *Clin Cancer Res.* **2005,** *11,* 6944-6949.

46 Tarantola, M.; Pietuch, A.; Schneider, D.; Rother, J.; Sunnick, E.; Rosman, C. Toxicity of gold-nanoparticles: synergistic effects of shape and surface functionalization on micromotility of epithelial cells. *Nanotoxicology.* **2011,** *5*, 254-268.

47 Timko, B. P.; Whitehead, K.; Gao, W.; Kohane, D. S.; Farokhzad, O.; Anderson, D. Advances in Drug Delivery. *Annu. Rev. Mater. Res.* **2011,** *41*, 1-20.

48 Liu, H. Y.; Chen, D.; Li, L. L.; Liu, T. L.; Tan, L. F.; Wu, X. L. Multifunctional gold nanoshells on silica nanorattles: a platform for the combination of photothermal therapy and chemotherapy with low systemic toxicity. *Angew. Chem. Int. Ed.* **2011,** *123*, 891-895.

Figure Legends

Figure 1: Illustration of AuNRs-PE-BSA formation, DOX encapsulation and release study.

Figure 2: A) The solution colors and morphologies of gold nanomaterials (a: Seed solution; b: aqueous solution of Au nanoparticels; c to e: AuNRs with different aspect ratios); **B)** AuNRs with the longitudinal surface plasmon resonance bands at 765 nm (a) and 808 nm (b); **C)** The TEM photo of as prepared AuNRs before centrifugation (a); (b) The TEM photos (× 50000) of as prepared AuNRs after centrifugation; (c) The TEM photos (× 75000) of as prepared AuNRs after centrifugation; (d) The TEM photos (× 100000) of as prepared AuNRs after centrifugation.

Figure 3: A) the high resolution TEM micrographs of the AuNRs coated by different layers (CTAB, PSS+PDDA+PSS+PDDA, PE); **B)** The UV-Vis-IR absorbance spectra of the AuNRs of different layers (CTAB, PSS+PDDA+PSS+PDDA, PE).

Figure 4: A) Zeta potentials of as-prepared AuNRs dispersed in aqueous solution; **B)** SDS-PAGE measurement of BSA adsorbed by various samples (1: marker; 2: AuNRs-PE; 3: AuNRs; 4: AuNRs-PE-BSA; 5: BSA); **C)** TGA curve of AuNRs-PE-BSA in the temperature range of 30 °C to 400 °C.

Figure 5: A) LCFM images of MCF-7 cells incubated with DOX, AuNRs/DOX-PE and AuNRs/DOX-PE-BSA for 45 min. Hoechst was used for nuclei staining; **B)** The LCFM images of MCF-7 cells incubated with AuNRs/DOX-PE-BSA at different time intervals (15 min, 35 min and 1 h).

Figure 6: A) In vitro cytotoxicity studies of AuNRs, AuNRs-PE-BSA and

AuNRs/DOX-PE-BSA performed on MCF-7 cell lines by MTT assays (incubation time: 24 h, n=6, $p < 0.05$); **B)** The cell inhibition rates of free DOX, free DOX with laser excitation, AuNRs/DOX-PE and AuNRs/DOX-PE-BSA with 765 nm laser irradiation (incubation time: 4 h, n=6, $p < 0.05$); **C)** The single or combined chemotherapeutic and thermotherapeutic effect of AuNRs/DOX-PE-BSA under NIR light were compared by the cell morphology and amounts, which was shown by the DIC mode of LCFM.

Figure 7: A) The NIR fluorescence images of the mice for control (before injection) and the mice treated with AuNRs/DOX-PE-BSA; **B)** The tissue distribution of DOX and AuNRs/DOX-PE-BSA after 16 days of intratumoral injection was demonstrated by the red fluorescence signals in heart and tumor.

Figure 8: Thermo- and chemo-therapeutic efficacy of AuNRs/DOX-PE-BSA in S180 tumor-bearing mice. **A)** The tumor volume of S180 tumor-bearing mice treated with PBS, PBS (NIR light), free DOX, free DOX (NIR light), AuNRs-PE-BSA (NIR light) and AuNRs/DOX-PE-BSA (NIR light), respectively; **B)** H&E stained tumor tissues of control mouse, AuNRs-PE-BSA (NIR light) group, free DOX group, AuNRs/DOX-PE-BSA (NIR light) group ; **C)** H&E stained tissue (heart, liver, spleen, lung and kidney) of control mouse and AuNRs/DOX-PE-BSA (NIR light) treated mouse, respectively.

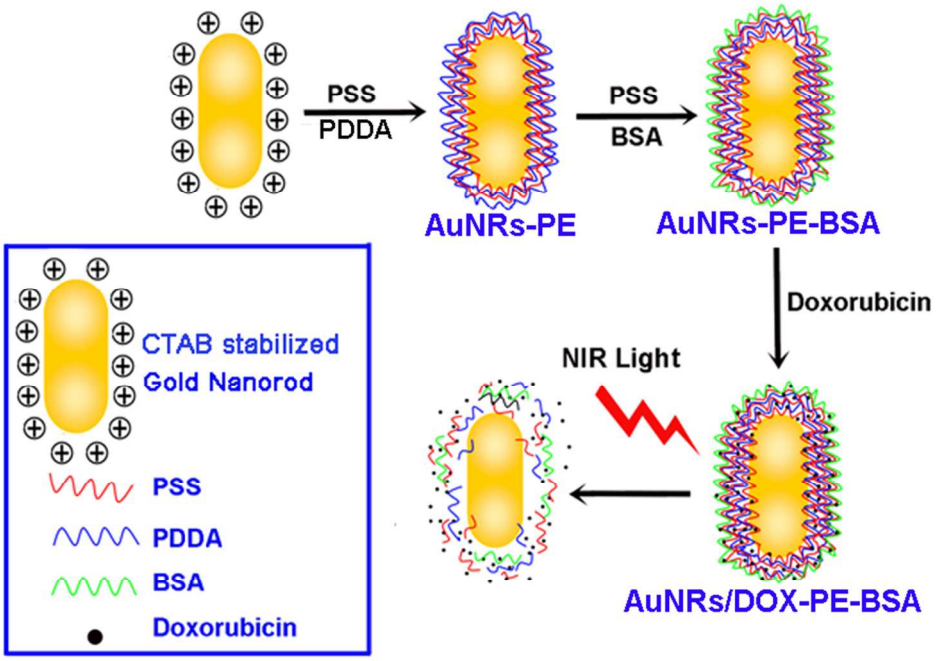

Figure 1: Illustration of AuNRs-PE-BSA formation, DOX encapsulation and release study.
80x54mm (300 x 300 DPI)

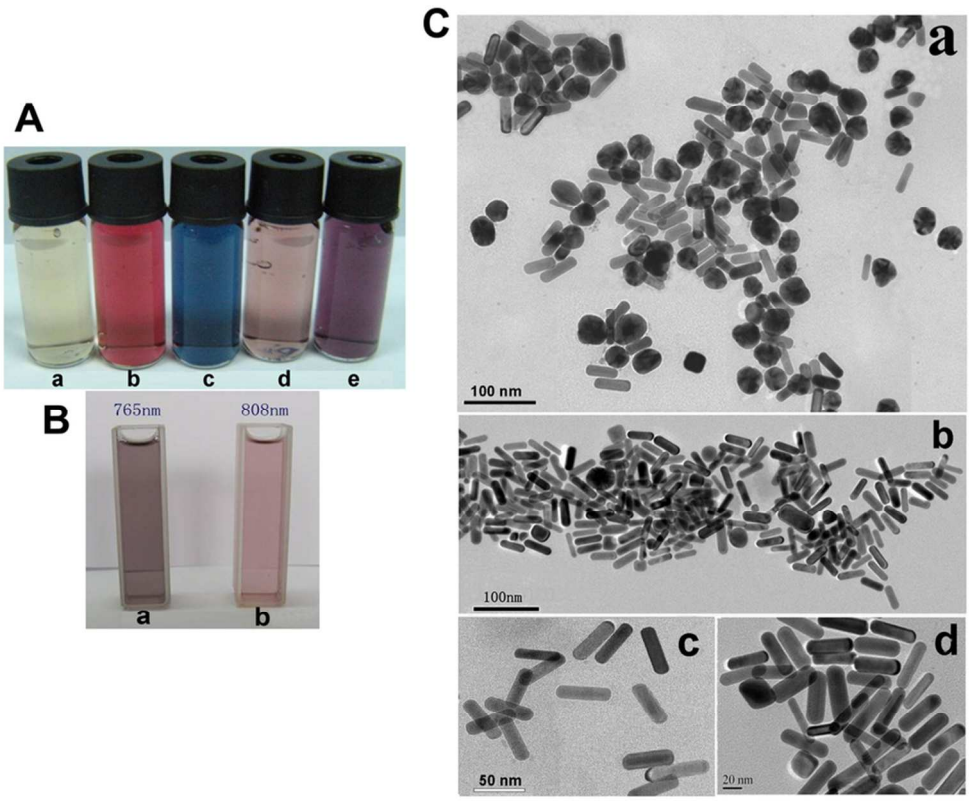

Figure 2: A) The solution colors and morphologies of gold nanomaterials (a: Seed solution; b: aqueous solution of Au nanoparticels; c to e: AuNRs with different aspect ratios); B) AuNRs with the longitudinal surface plasmon resonance bands at 765 nm (a) and 808 nm (b); C) The TEM photo of as prepared AuNRs before centrifugation (a); (b) The TEM photos (× 50000) of as prepared AuNRs after centrifugation; (c) The TEM photos (× 75000) of as prepared AuNRs after centrifugation; (d) The TEM photos (× 100000) of as prepared AuNRs after centrifugation.
80x65mm (300 x 300 DPI)

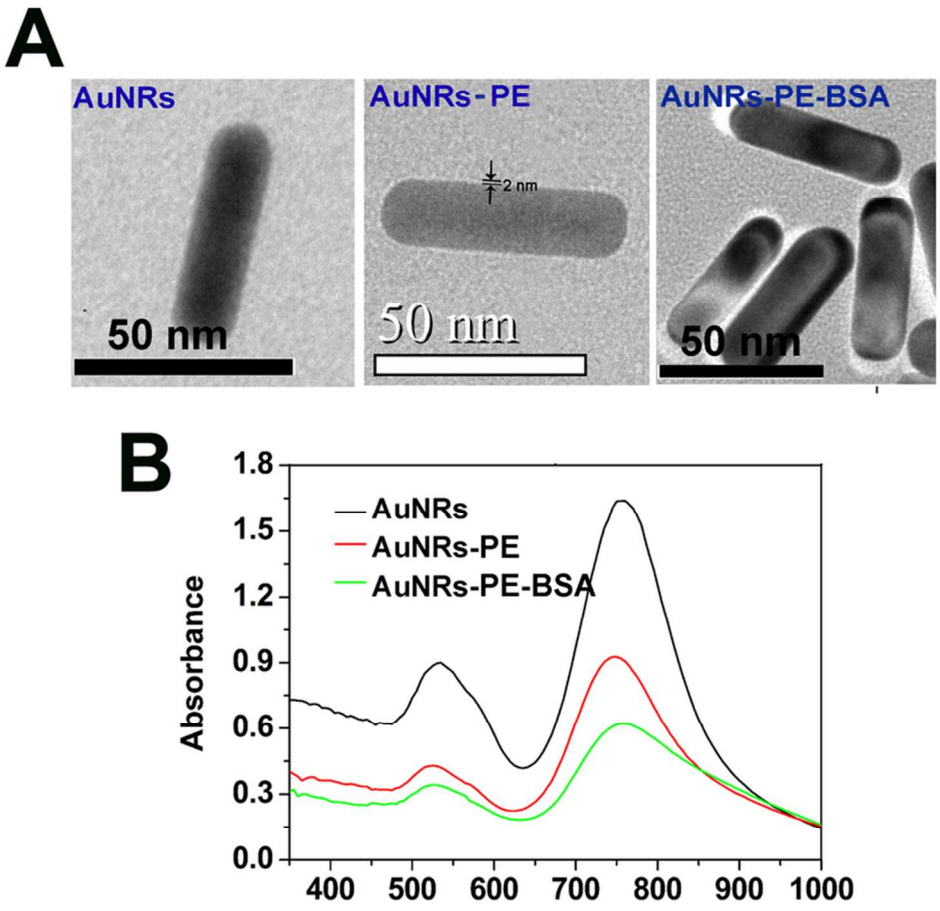

Figure 3: A) the high resolution TEM micrographs of the AuNRs coated by different layers (CTAB, PSS+PDDA+PSS+PDDA, PE); B) The UV-Vis-IR absorbance spectra of the AuNRs of different layers (CTAB, PSS+PDDA+PSS+PDDA, PE).
75x71mm (300 x 300 DPI)

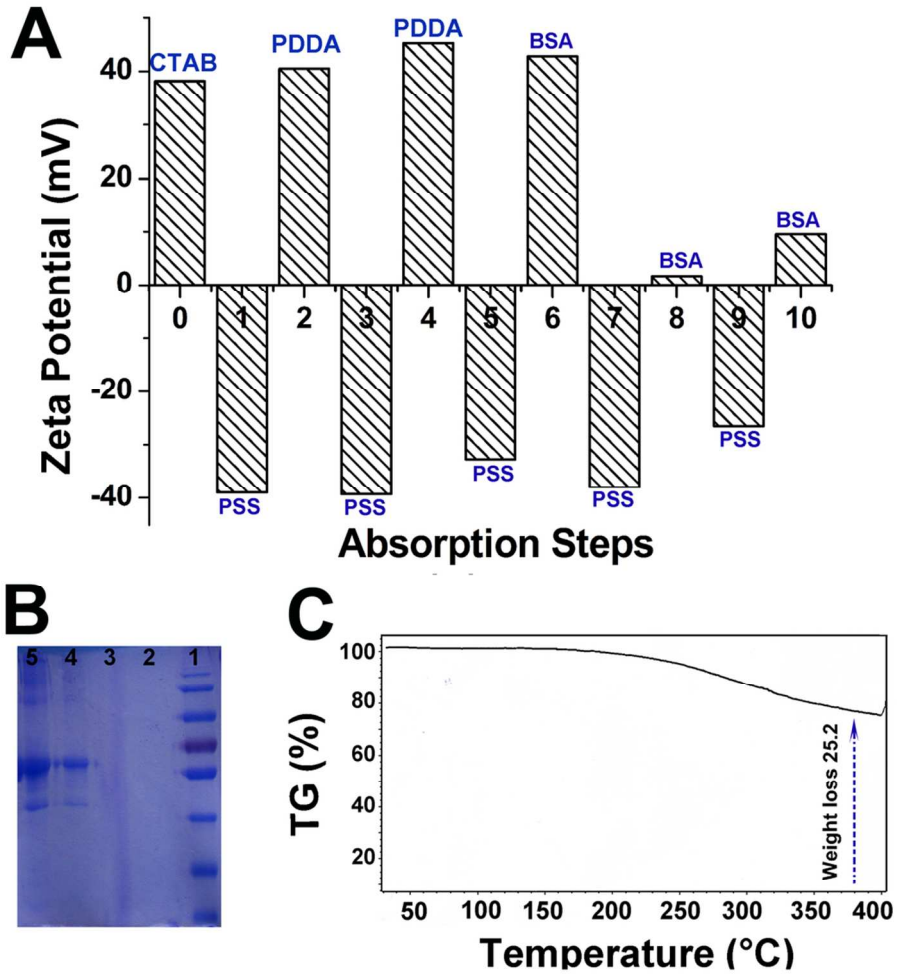

Figure 4: A) Zeta potentials of as-prepared AuNRs dispersed in aqueous solution; B) SDS-PAGE measurement of BSA adsorbed by various samples (1: marker; 2: AuNRs-PE; 3: AuNRs; 4: AuNRs-PE-BSA; 5: BSA); C) TGA curve of AuNRs-PE-BSA in the temperature range of 30 °C to 400 °C.
98x96mm (300 x 300 DPI)

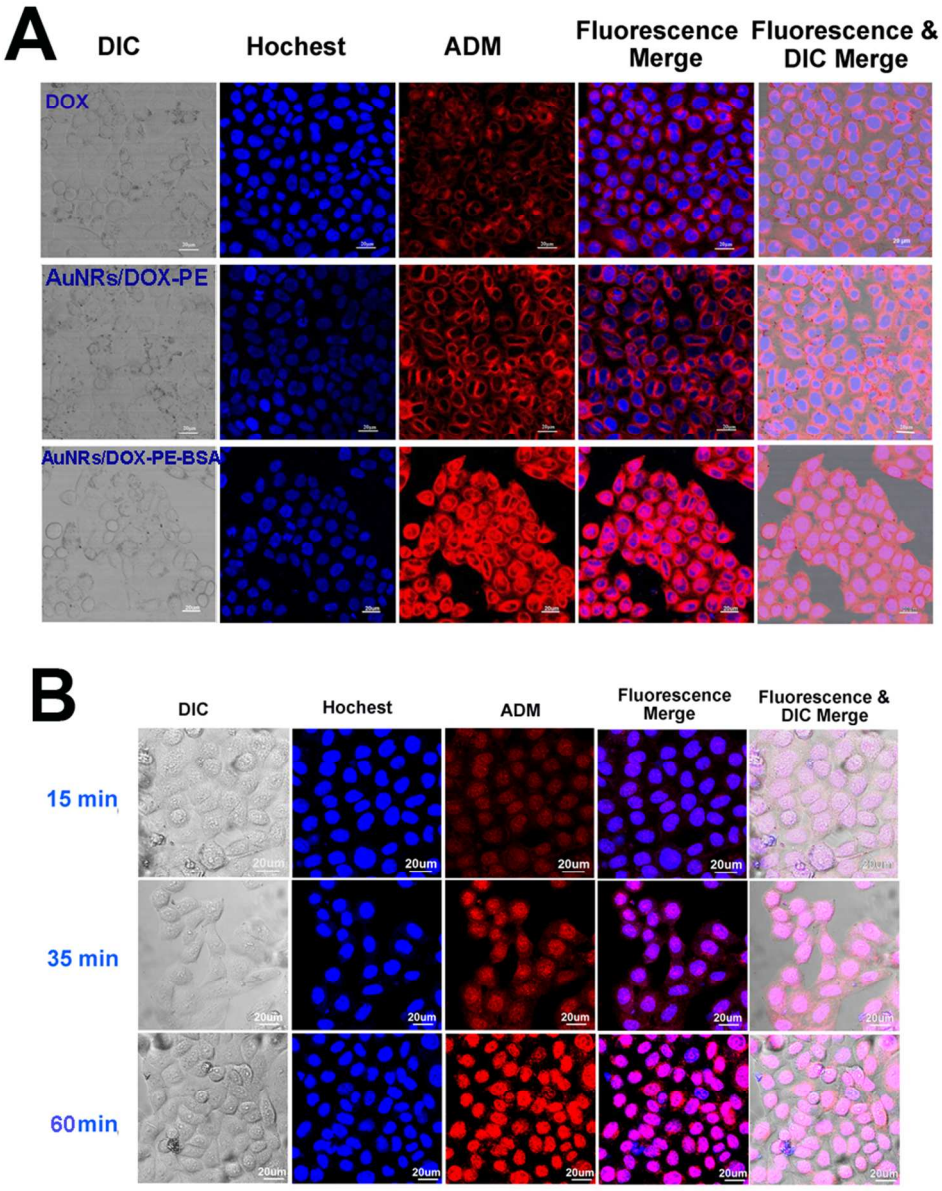

Figure 5: A) LCFM images of MCF-7 cells incubated with DOX, AuNRs/DOX-PE and AuNRs/DOX-PE-BSA for 45 min. Hoechst was used for nuclei staining; B) The LCFM images of MCF-7 cells incubated with AuNRs/DOX-PE-BSA at different time intervals (15 min, 35 min and 1 h).
85x104mm (300 x 300 DPI)

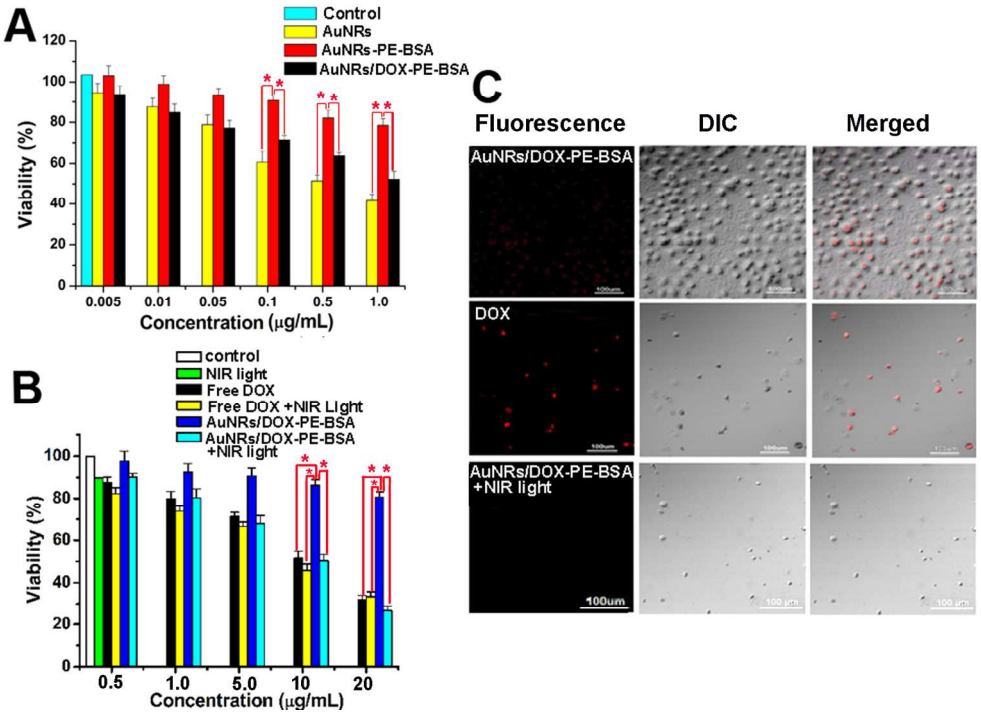

Figure 6: A) In vitro cytotoxicity studies of AuNRs, AuNRs-PE-BSA and AuNRs/DOX-PE-BSA performed on MCF-7 cell lines by MTT assays (incubation time: 24 h, n=6, $p < 0.05$); B) The cell inhibition rates of free DOX, free DOX with laser excitation, AuNRs/DOX-PE and AuNRs/DOX-PE-BSA with 765 nm laser irradiation (incubation time: 4 h, n=6, $p < 0.05$); C) The single or combined chemotherapeutic and thermotherapeutic effect of AuNRs/DOX-PE-BSA under NIR light were compared by the cell morphology and amounts, which was shown by the DIC mode of LCFM.
150x107mm (300 x 300 DPI)

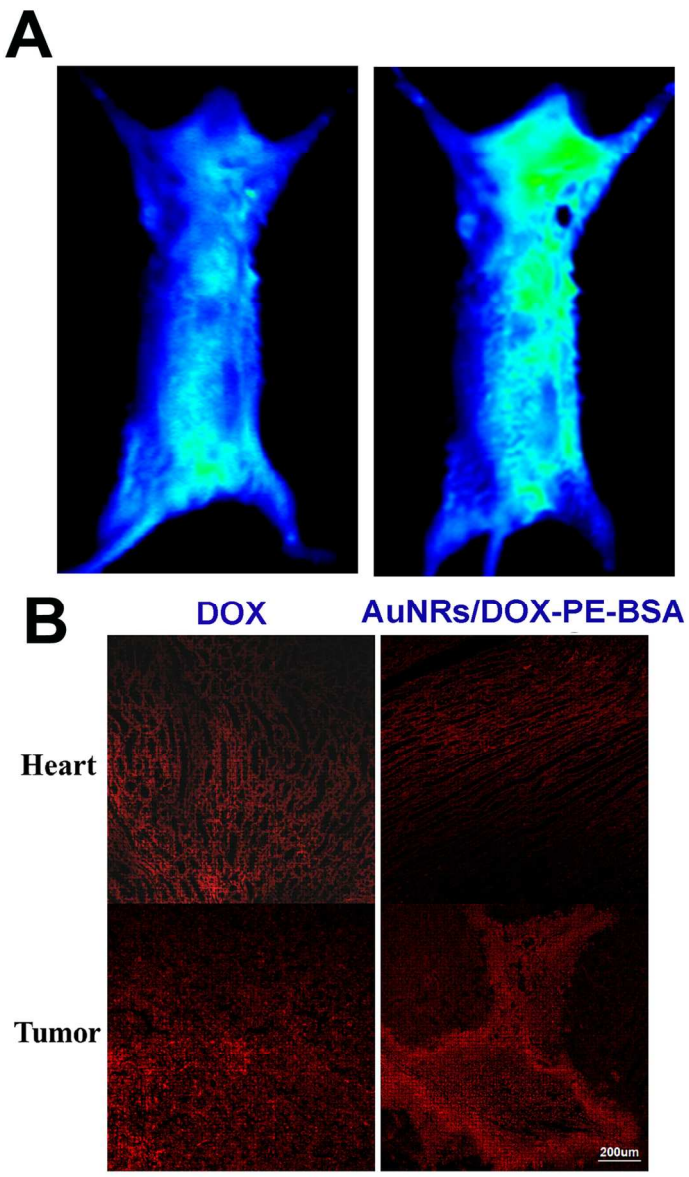

Figure 7: A) The NIR fluorescence images of the mice for control (before injection) and the mice treated with AuNRs/DOX-PE-BSA; B) The tissue distribution of DOX and AuNRs/DOX-PE-BSA after 16 days of intratumoral injection was demonstrated by the red fluorescence signals in heart and tumor.
103x176mm (300 x 300 DPI)

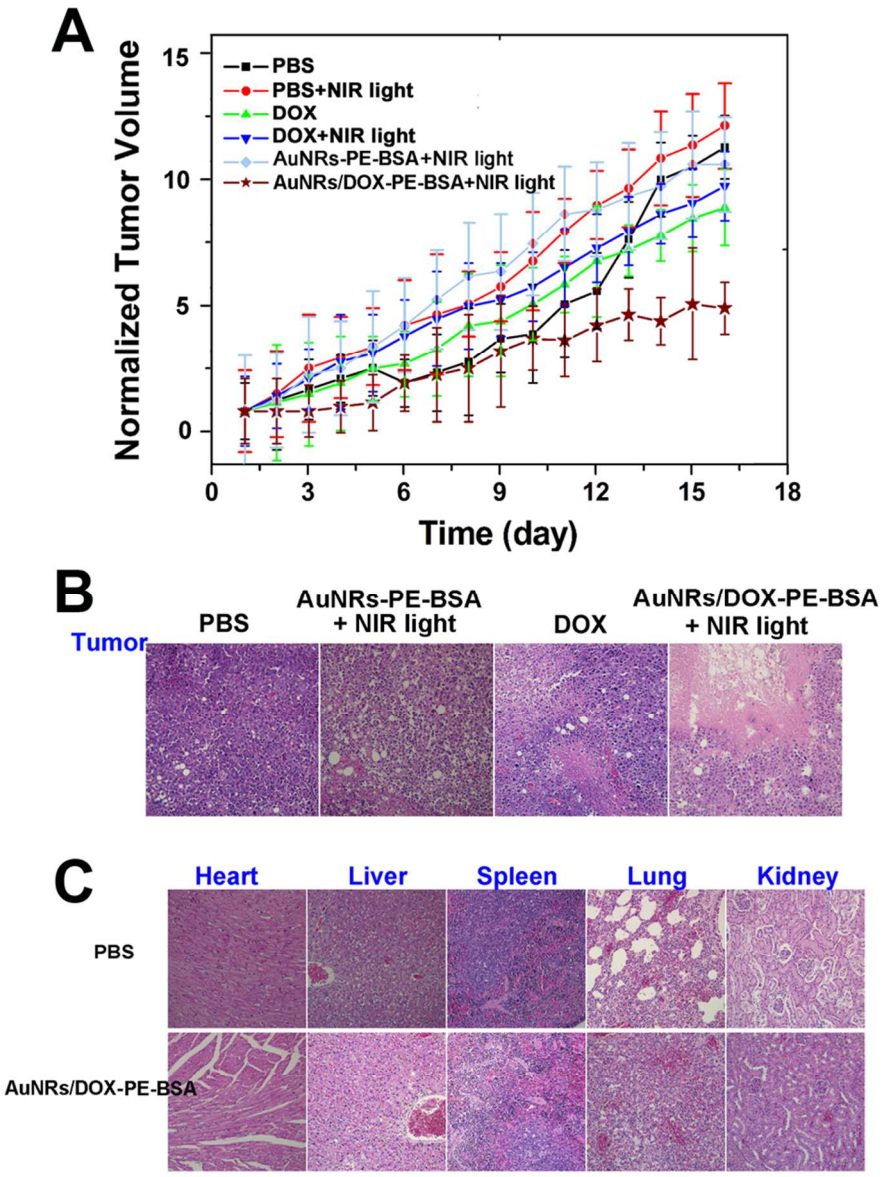

Figure 8: Thermo- and chemo-therapeutic efficacy of AuNRs/DOX-PE-BSA in S180 tumor-bearing mice. A) The tumor volume of S180 tumor-bearing mice treated with PBS, PBS (NIR light), free DOX, free DOX (NIR light), AuNRs-PE-BSA (NIR light) and AuNRs/DOX-PE-BSA (NIR light), respectively; B) H&E stained tumor tissues of control mouse, AuNRs-PE-BSA (NIR light) group, free DOX group, AuNRs/DOX-PE-BSA (NIR light) group ; C) H&E stained tissue (heart, liver, spleen, lung and kidney) of control mouse and AuNRs/DOX-PE-BSA (NIR light) treated mouse, respectively.
80x109mm (300 x 300 DPI)

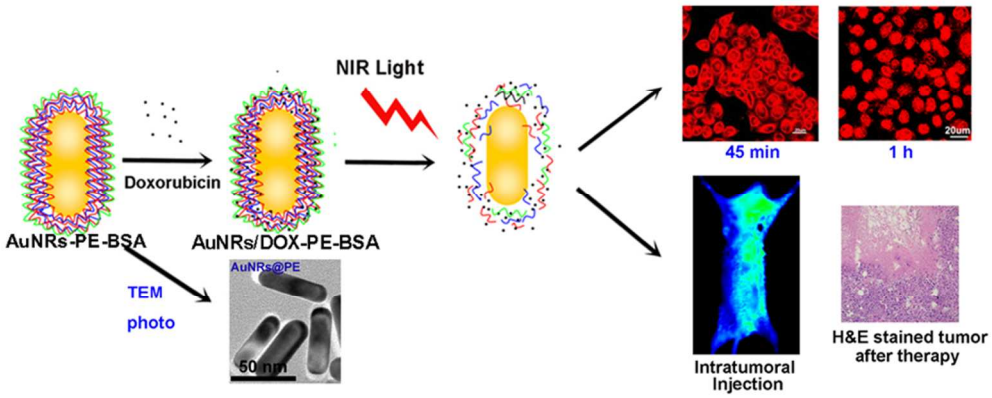

Graphic Abstract: Drug loaded multi-layered gold nanorods exhibited synergistic photothermal and chemotherapy effect on tumor.

80x32mm (300 x 300 DPI)